Characteristics of phosphate adsorption on ferric hydroxide synthesized from a Fe$_2$(SO$_4$)$_3$ aqueous solution discharged from a hydrometallurgical process

Ho-Sung Yoon*, Kyung Woo Chung*, Chul-Joo Kim*, Jin-Ho Kim**, Hyung-Seop Lee**, Seok-Jong Kim***, Se-Il Lee**, Seung-JoonYoo**,†, and Byung-Chul Lim****

*Korea Institute of Geoscience & Mineral Resources (KIGAM), 124 Gwahang-ro, Yuseong-gu, Daejeon 34132, Korea
**Department of Biomolecular and Chemical Engineering, Seonam University, 7-111 Pyeongchon-gil, Songak, Asan 31556, Korea
***Department of Environmental and Chemical Engineering, Seonam University, 439 Chunhayng-ro, Namwon 55724, Korea
****Sunglim Rare Earth Metal Co., 8 Holim, Daegu 42714, Korea

Abstract–Ferric hydroxide adsorbent was prepared by a chemical treatment process with H$_2$O$_2$, NaOH, and aeration from a Fe$_2$(SO$_4$)$_3$ aqueous solution as a side product discharged from the hydrometallurgical process used to extract neodymium. The ferric hydroxide was used as an adsorbent to prevent eutrophication in water. At the time of synthesis, the most important process variable is the pH condition, which, in this experiment, was changed from pH 3 to 13. The cost of synthesizing ferric hydroxide was sharply reduced by using ferric sulfate, which is considered a side product of the aforementioned hydrometallurgical process, as a starting material, and an adsorbent with high adsorption ability was prepared by controlling the pH level. Microstructural characterization of the synthesized ferric hydroxide revealed particles with a specific surface area of 194.2 m^2/g and an average pore diameter of 2.66 nm at pH 6 and 298 K. A column-type packed-bed adsorption experiment was conducted under the following conditions: a flow rate of 0.567 BV/min (3.2 mL/min), 298 K, and atmospheric pressure. The results of the adsorption performance test indicated that the adsorption efficiency of phosphate at concentrations of 10 ppm was 100% at a flow rate of 0.567 BV/min within a contact time of 2 min, and the maximum adsorption capacity for phosphate ions was 65 mg/g.

Keywords: Phosphate, Adsorption, Ferric Hydroxide, Eutrophication

INTRODUCTION

Recent years have seen frequent occurrences of blue-green algal blooms in the rivers and lakes of South Korea. This has become a severe problem nationally, and has affected the environment adversely. The main causes of the algal blooms are the water temperature, sunlight, flow rate of water, and the presence of nutrients in water. Among these factors, the air temperature is difficult to control artificially and the flow rate of water in rivers and lakes is also difficult to control. Accordingly, the only controllable variable is the removal of nutrients from the water to avoid the occurrence of algal blooms in rivers and lakes.

Commonly, it has been assumed that eutrophication of rivers and lakes is only limited by P, and that of marine systems is limited by N. Recently, the consensus is that the phosphate is generally the most limiting nutrient in aquatic ecosystems [1,2].

The mechanism whereby blue-green algae occur and the consequences thereof can be expressed as shown in Fig. 1, which shows that phosphorus is an important key factor causing blue-green algae. Phosphorus results in eutrophication increase in the nutrients in water, after which the eutrophication rapidly leads to the proliferation of the blue-green algae. As a result, the algae can explode into
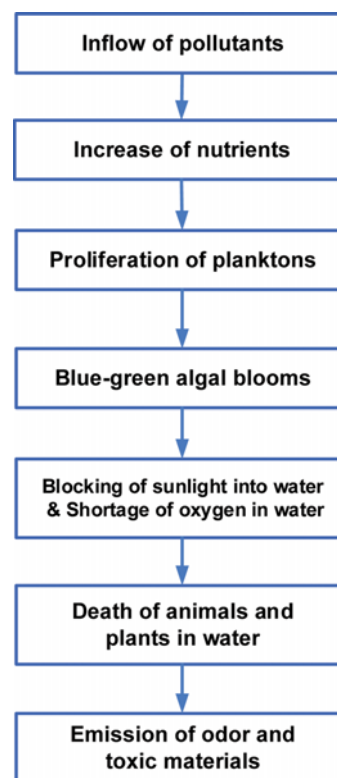

Fig. 1. Cause-and-effect mechanism of algal blooms.

†To whom correspondence should be addressed.
E-mail: sjyoo001@hanmail.net

macro-algal blooms in rivers and lakes. These algal blooms have the effect of reducing the dissolved oxygen in water. Eventually, insufficiency of this dissolved oxygen leads to the death of animals and plants in rivers and lakes, thereby restricting the use of the polluted water for drinking, agricultural, and even industrial purposes.

Accordingly, the prevention of algal blooms requires us to prevent nutrients from flowing into the water. Many methods such as filtration, membranes, reverse osmosis, chlorination oxidation, electro-coagulation, precipitation, ion exchange, and biological treatment, have been developed to control the inflow of nutrients. Although each of these methods has its advantages and disadvantages, generally, these technologies have inherent limitations such as poor efficiency, sensitive operating conditions, costly equipment, and the production of a sludge incurring additional expense [3].

In this study, we used an adsorption technology that is relatively simple and economical compared to the above-mentioned technologies. Adsorption has been a promising technique owing to its advantages including simplicity, low cost, high efficiency, limited production of sludge, and its ease of operation and maintenance [4]. Admittedly, adsorption also has its disadvantages, but we focused on overcoming the limitations.

The key aspect of adsorption is the development of an inexpensive adsorbent with high absorption ability. Our approach involved selecting ferric hydroxide for use as the adsorbent. Ferric hydroxide was prepared from ferric sulfate, which is a side product discharged from the hydrometallurgical process used for the extraction of neodymium. The ferric sulfate is considered and treated as waste exhausted from the metal leaching process. Thus, the raw material is easy to obtain and the cost to produce the adsorbent is lower than that of all the other adsorbents.

Table 1. Efficiency of phosphate removal by various adsorbents

Ads. type	Raw material	Adsorbent	Surface area (m^2/g)	Adsorbent dosage (g/L)	Max. phosphate adsorption capacity (mg/g)	Initial phosphate conc. (mg/L)	Contact time (min)	pH/ T (K)	Analysis	Adsorption efficiency (%)	Ref.
Batch	Chitosan, $ZrOCl_2$	CCP-Zr		0.1	71.68	100	20	3/30, 40, 50		97.8	4
Batch	S. Purpurea fruit	S-NaOH Nanoscale Zerovalent iron (NZVI)	-	0.25 0.5	130	19 45 150	5	4	ICP-AES	99.9 88.3 86.0	5
Batch	Tourmaline, $LaCl_3$	La-tourmaline	15.59	1	108.7	5	15	7		90	6
Batch	$Mg(OH)_2$, bentonite	Mg-modified bentonite	33.52	2	14.33	25	120	7	UV-VIS	>54	7
Batch	ZrO_2 Fe_2O_3	ACF-ZrFe	1300-1400	1	26.3	10-30	1400	4	UV-Vis	77	8
Batch	Natural zeolite	$Ca(OH)_2$-Zeolite	-	10	7.57	10	120 h	7	Ascorbic acid	97.6	9
Batch	$ZrOCl_2$, $Fe_2(SO_4)_3$	Zr-Iron oxide (MZIO)	282	2	21.3	5-100	40 h	4	Ammonium molybdate/ UV-Vis	60-70	10
Batch	Chitosan, $CuSO_4$	Cu-CS			28.86	100	400	5/25	UV-Vis	99	11
Batch	$FeCl_3$ $ZrOCl_2$	Fe-Zr Oxide	339	0.2	33.4	10	90	5.5	ICP-AES	93	12
Batch & Column	Zeolite	Zeolite ball coated with sulfate (ZBCS)	9.3831	0.25	15.13	50	12 h	4.76	IC	-	13
Batch	$Al_2(SO_4)_3$, $KMnO_4$, $MnCl_2$, AlOOH	Mn oxide doped Al oxide (MODAO)		0.2	59.8	2-45	5 h	6	ICP-AES		14

In conventional adsorption technologies, various adsorbents have been used for the removal of phosphate such as sands, fly ash, steel slag, red mud, zeolite, activated alumina, ferric hydroxide, limestone, gypsum, calcite, bentonite clay, diatomite, and polymer hydrogels. Each of these adsorbents has its advantages and disadvantages. Table 1 summarizes the various adsorbents for the removal of phosphate.

Among these adsorbents, nanoscale zerovalent iron (NZVI) [5], CCP-Zr [4], and La-loaded tourmaline, were shown to exhibit high adsorption efficiency and maximum adsorption capacity [6]. Especially, the NZVI adsorbent has a high efficiency of 99.9% and a maximum absorption capacity of 130 mg/g for an adsorbent dosage of 0.25 g/L. The CCP-Zr adsorbent has a maximum absorption capacity of 71.68 mg/g for an adsorbent dosage of 0.1 g/L. La-loaded tourmaline has a high efficiency of 90.0% and maximum absorption capacity of 108.7 mg/g for an adsorbent dosage of 1.0 g/L. The adsorbent with the highest maximum adsorption characteristic to date appears to be NZVI. However, suitability for application in the field is not only determined by properties such as the maximum adsorption capacity, which is not a unique standard to indicate whether an adsorbent would be excellently suited for practical implementation. In this respect, a low production cost and easiness of large-scale production would be equally important.

Although the adsorbents listed in Table 1 have very good adsorption characteristics, they commonly have poor economic viability because they require the use of expensive raw materials. Lee et al. presented the results of evaluation of economics on the removal and recycling of phosphate, and they showed their high unit costs of 82-1,750$ for 1 g P removal [15].

Accordingly, we targeted the preparation of an adsorbent with excellent economic performance and adsorption ability. In respect of economic viability, aqueous ferric sulfate is highly appropriate because it is a side product discharged from the aforementioned hydrometallurgical process.

In the end, if the ferric sulfate could be used to prepare an adsorbent with excellent adsorption ability, it would be optimal as it would meet all our requirements as an adsorbent.

EXPERIMENTAL

1. Materials

The ferric sulfate aqueous solution used as the raw material was a side product of the sulfuric acid ($2.5 M H_2SO_4$, 98%, Merck) leaching process that is used to recover neodymium from NdFeB magnets (slurry density of 500 g NdFeB/L).

The initial pH of ferric sulfate solution used as a raw material was shown as 0.005.

Ferric hydroxide was synthesized by the chemical treatment of this $Fe_2(SO_4)_3$ aqueous solution as follows: a $Fe_2(SO_4)_3$ solution of 1 L was reacted with hydrogen peroxide (H_2O_2, 30%, Merck) at 50 °C and an impeller speed of 300 rpm using the double-jacketed Pyrex reactor. A stoichiometric ratio of H_2O_2 was slowly added in small portions to 1 mol $Fe_2(SO_4)_3$ solution to prevent the reactants from overflowing due to the occurrence of effervescence by rapid oxidation. During H_2O_2 oxidation, air was continuously introduced into the reactor by an air pump to convert the ferrous

hydroxide to ferric hydroxide. In this synthetic reaction of ferric hydroxide, the most important process variable was the pH condition, which was controlled to remain within the range of 3 to 13. The desired pH was obtained by using sodium hydroxide (NaOH, 99%, Merck). After the desired pH was attained, the solution was maintained aerated for a period of 24 hours. The ferric hydroxide prepared in this reaction was adequately washed by distilled water and the solid precipitates were separated from the liquid by centrifugation for 5 min at 3,500 rpm. The process was repeated five times. The solid powder separated by centrifugation was dried for 3 days at 70 °C. The dried solid powders were milled with a mortar and pestle. Finally, the solid powder was classified into granules with a size of 1-2 mm and used as the adsorbent.

2. Adsorption Performance Test

A phosphate solution (10 ppm) was prepared using ortho-phosphoric acid (H_3PO_4, 85.00%, Merck). The adsorption performance test was conducted using the column-type adsorption apparatus with 13 mm inside diameter as shown in Fig. 2 because it is easier to apply a column-type fixed bed reactor in commercial adsorption apparatus than a batch reactor. To compare the maximum adsorption amounts and adsorption efficiency between column-type adsorption and batch-type adsorption, batch-type adsorption experiment was also carried out for the adsorption performance test.

A sieve was used to classify the dried ferric hydroxide powder to a particle size of 1-2 mm. For the column-type adsorption experiment, ferric hydroxide of 5 g was added from the top of the column onto the bed filter. The reactor was designed with an open-end to the atmosphere to induce downward flow by using the

Fig. 2. Schematic diagram of column-type packed-bed adsorption reactor.

potential energy of gravity as shown in Fig. 2. A phosphate solution of 10 ppm was injected into the upper zone of the column at a flowrate of 0.567 BV/min a peristaltic pump at 298 K. Different concentrations of the phosphate effluent gathered in the reservoir from the U-type column after passage through the ferric hydroxide-packed bed by gravity and analyzed by ICP-AES.

3. Analysis

Many analytical methods as shown in Table 1 have been used to analyze the phosphate concentration but ICP-AES (inductively coupled plasma-atomic emission spectrometry, *i*CAP6000, Thermo Fisher, UK) was selected for the credible analysis on the phosphate ion [18,19]. The wavelength for ICP-AES analysis was selected as 213.6 nm and the RF power was 1,350 W, at which interference between the elements is minimized. The standard solution that was used for ICP-AES was a phosphate standard solution traceable to SRM (Standard reference material) from NIST, which was KH_2PO_4 in H_2O of Merck. The amounts of adsorbed water and structural water were analyzed from room temperature to 1,300 °C at a heating rate of 20 °C/min and under an N_2 atmosphere by using a TG-DTA analyzer (STA 709 PC, Netzsch). The pH values were measured by using the pH electrode of an advanced electrochemistry meter (Orion VERSASTAR, Thermo Scientific). The morphology of the particles was observed as a function of pH by using a scanning electron microscope (15 kV, JEOL, JSM-6400). Nitrogen adsorption and desorption was measured at 77 K using a Micromeritics TriStar 3000 automatic analyzer after the sample was degassed for 2 h in the degas port of the adsorption apparatus.

In many previous studies, the PZC (point of zero charger) of the adsorbent was determined by using a zetapotential measuring analyzer by electrophoresis, but the pH range of PZC can be wide. In this experiment, we measured the final pH after the input of adsorbent to the initial pH condition and enough shaking of 2 h. This is necessary because the final pH undergoes a shift and differs from the initial pH caused by a proton either being taken up or released according to the surface hydroxyl groups of the adsorbents. This phenomenon is visualized by using a pH shift diagram. When using this diagram for measuring purposes, it is more convenient to use the PZC of the adsorbent than the zetapotential measuring device. In this experiment, the PZC of the synthesized adsorbent was found to be 5.7 and the pH range of PZC appeared over a wide range of pH 3 to 12. Therefore, the adsorption of phosphate occurred under conditions below pH 4 and desorption took place above pH 12. Additionally, the pH of the solution was adjusted by hydrochloric acid (HCl) and sodium hydroxide (NaOH) solution to attain the desired pH value.

RESULTS AND DISCUSSION

1. Synthesis of Adsorbent

The ferric hydroxide adsorbent was prepared by using ferric sulfate discharged from the hydrometallurgical process as a raw material. The elemental composition of ferric sulfate used as a raw material in this experiment was analyzed by ICP-MS as shown in Table 2.

If the ferric sulfate solution is converted into the ferric hydroxide which is characterized by high adsorption as proposed in the

Table 2. Elemental composition of ferric sulfate by ICP-MS

Element	Fe	Pr	Nd	Tb	Dy	Sum
Conc.	99.90%	0.02%	0.04	0.00%	0.01%	100%

Pourbaix diagrams [16,17], the synthesized ferric hydroxide will be considered as a good adsorbent in the respects of low production cost, ease of large-scale production.

Recently, the national water quality standard for Class I water resources in South Korea, has been below 0.01 ppm in lakes. This strengthened standard requires a highly efficient adsorbent. Accordingly, we targeted the preparation of material of ferric hydroxide with a good adsorption characteristic on the phosphate.

This ferric sulfate was first oxidized by the addition of H_2O_2 and the pH of the resulting solution was adjusted to the desired value using sodium hydroxide. After pH control, the solution was continuously purged with air for 24 h to convert the ferrous hydroxide to ferric hydroxide, which precipitated from the solution. This precipitate was dried at 70 °C and was milled using a mortar and pestle.

Fig. 3 shows the XRD patterns of ferric hydroxide powder as a function of the pH. The result of the XRD analysis showed that the precipitate synthesized at pH 6 was ferric hydroxide powder with an amorphous structure and partly magnetite crystalline structure. In contrast, the powder synthesized at pH 3 was considered to have a natrojarosite crystalline structure by JCPDS card, whereas the sample powder obtained at pH 9 mainly had the goethite structure and that obtained at pH 13 showed an amorphous structure with a small amount of goethite structure.

Fig. 4 shows the result of the TG-DTA analysis of the ferric hydroxide powder synthesized at pH 6 selected as an adsorbent. This analysis revealed two endothermic peaks: an endothermic peak at 100-270 °C and an endothermic peak at 550-850 °C. Moreover, another endothermic peak at temperatures exceeding 1,150 °C is considered an endothermic peak due to the conversion of $Fe(OH)_3$
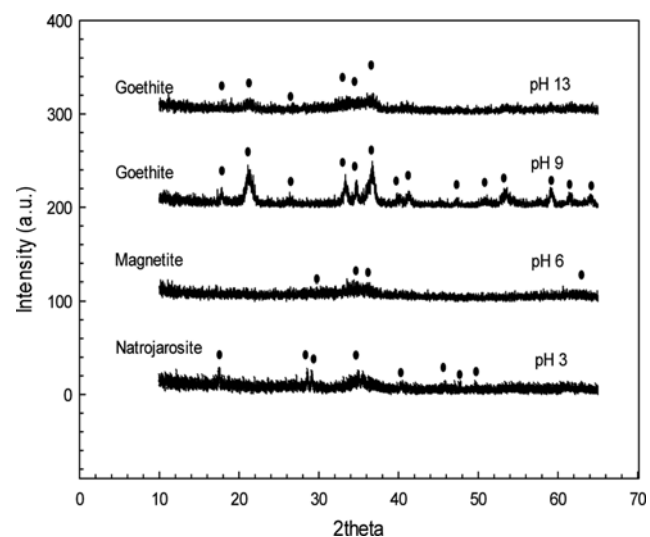

Fig. 3. XRD pattern of samples under different pH conditions: (a) pH 3 (b) pH 6 (c) pH 9 (d) pH 13.
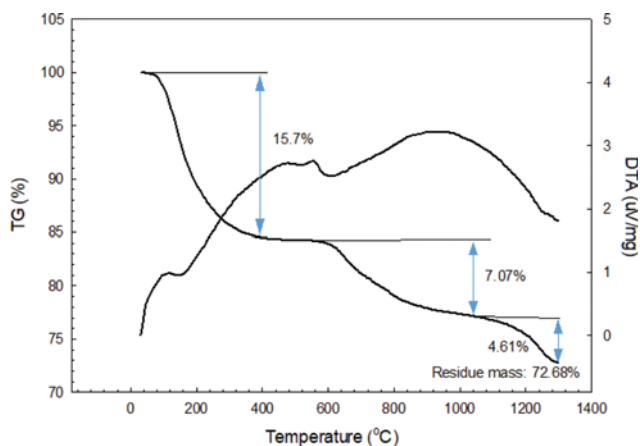
Fig. 4. DTA-DTA result of ferric hydroxide powders synthesized at pH 6.

to Fe_2O_3. In addition, the TG results indicated that the amount of adsorbed and structural water was 15.7% and 11.68%, respectively. These mass losses are considered as such that $Fe(OH)_3$ is first changed to Fe_3O_4 (magnetite structure) in the range of 550-850 °C and then Fe_3O_4 is converted into anhydrous Fe_2O_3 in the temperature range exceeding 1,150 °C.

The results of the N_2 adsorption and desorption analysis showed that the BET surface area of the ferric hydroxide synthesized at pH 6 was measured to the largest value of 194 m^2/g among the various pH conditions shown in Table 3. As shown in the adsorption/desorption isotherms and average pore diameters in Fig. 5, the average pore size was 2.7 nm and the pore volume was 0.129 cm^3/g, as calculated by the BJH method. Moreover, the sample powder obtained at pH 6 was shown to have the most appropriate microstructural characterization than any of the powder samples obtained under other conditions (pH 3, pH 9, and pH 13).

Samples shown in Table 3 show the ferric hydroxide powders synthesized by changing the pH conditions. The color of adsorbents appears yellow-brown at pH 3, almost black at pH 6, a reddish black at pH 9, and a dark reddish black at pH 13. Especially, it is impossible to use an adsorbent for the removal of phosphate by column-type packed-bed adsorption reactor because the Natro-

jarosite powder synthesized at pH 3 showed dissolution in water.

In this experiment, the powder synthesized at pH 6 was used in the column adsorption experiment and classified to the size of 1-2 mm by using a sieve to prevent the phosphate aqueous solution from clogging the column and to induce spontaneous flow by gravity.

In the case of pH 9, the specific surface area was smaller than that at pH 6 and the pore diameter was increased to 17 nm. The adsorbent obtained under these conditions did not have the requisite pore structure for phosphate adsorption. Meanwhile, in the case of pH 13, the specific surface area sharply decreased with a wide range of pore size distributions. Accordingly, passage of the phosphate solution through the large mesopores did not promote adsorption.

The N_2 adsorption-desorption isotherms of ferric hydroxides synthesized by changing the pH conditions are plotted in Fig. 5. The average pore size and pore volume were calculated by the BJH method. Hysteresis attributable to the mesoporous structure appeared at pH levels, as shown in Fig. 5. However, among these levels, the pore size distribution was highly uniform at pH 6. In addition, we could determine from the hysteresis that the pore has an ink-bottle-type structure.

Accordingly, we selected a sample synthesized at pH 6 as the adsorbent for the removal of phosphate. The PZC of the sample was obtained by measuring the equilibrium pH at high oxide loading (EpHL) as shown in Fig. 6. This sample had a PZC value of 5.7.

The surface potential indicated that ferric hydroxide has a positively charged surface in the case of pH<4 and a negatively charged surface in the case of pH>12. Therefore, ferric hydroxide adsorbent would be capable of strongly adsorbing the phosphate ion because it maintains a negatively charged ferric hydroxide surface potential at pH 4 in the case of a phosphate solution of 10 ppm. In addition, as shown in Fig. 6, if the solution maintains the condition above pH 12 in the case of desorption, the phosphate ions adsorbed on the surface of ferric hydroxide would be easily desorbed [20-28].

Generally, the phosphate adsorbed on the adsorbent can be desorbed by repulsive force through the control of the surface charge of the adsorbent. To induce the repulsive force between the surface charge of adsorbent with a cation and the phosphate ion with

Table 3. Physical properties of samples as a function of pH

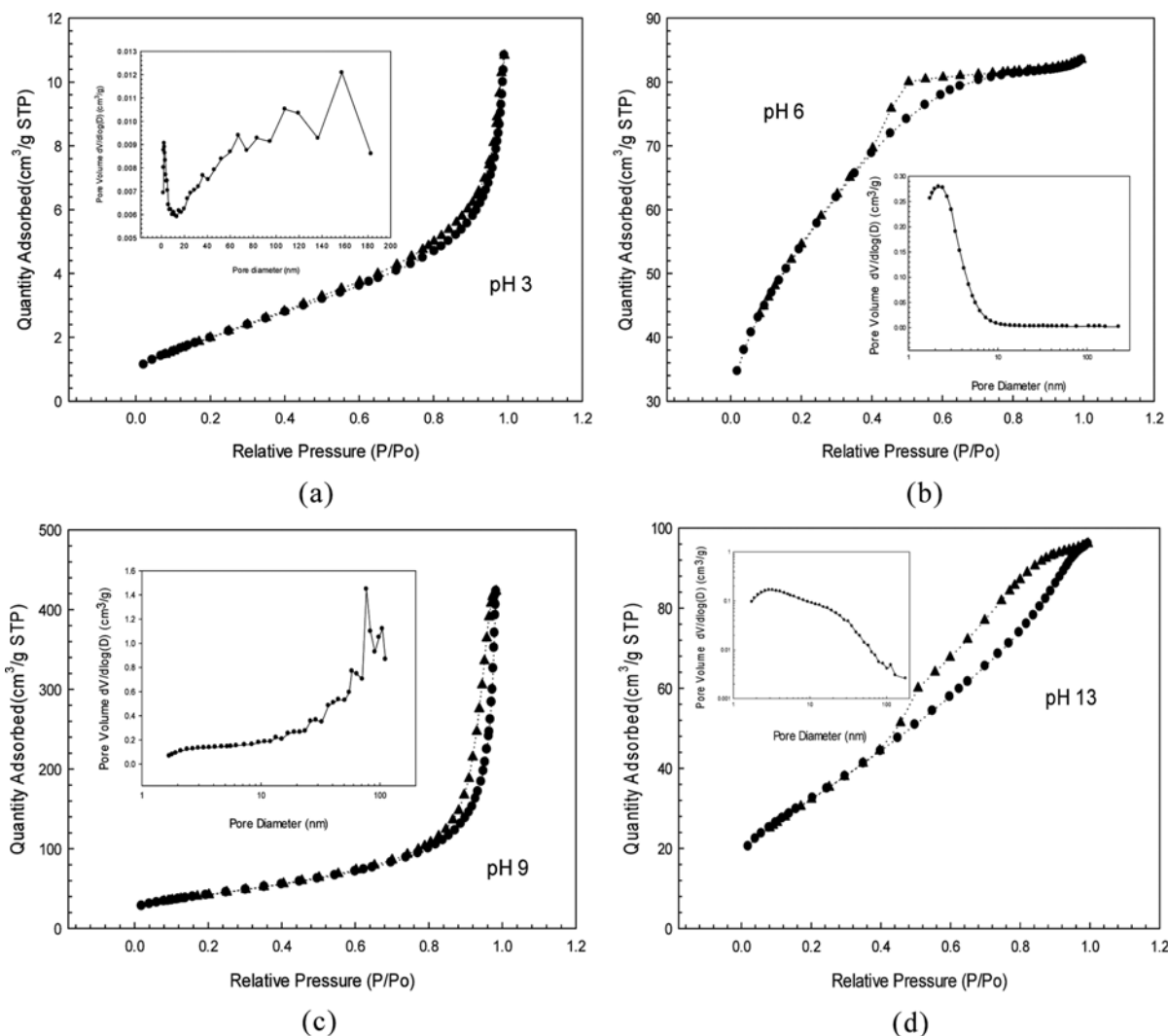| Characteristics	pH 3	pH 6	pH 9	pH 13
Surface area (BET), m^2/g	7.2	194.2	150.5	115.6
Pore volume, cm^3/g	0.017	0.129	0.654	0.148
Average pore size, nm	-	2.66	-	-
Synthesized sample				
Color	Yellow-brown	Black	Reddish black	Dark reddish black

Fig. 5. Isotherm plots and pore size distribution of ferric hydroxide samples obtained by changing the pH: (a) pH 3 (b) pH 6 (c) pH 9 (d) pH 13.
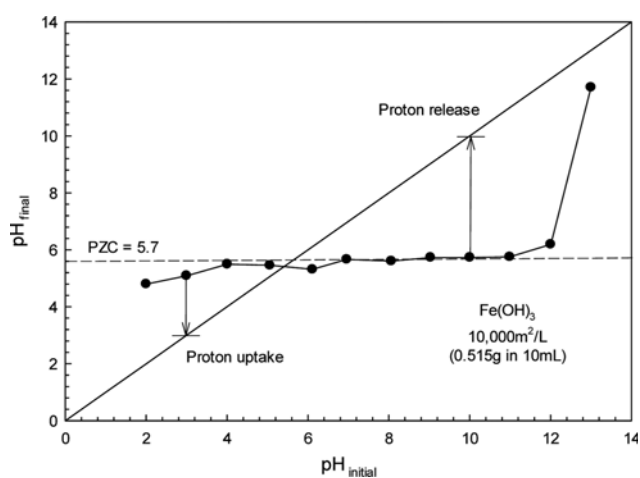

Fig. 6. EpHL measurement of PZC of ferric hydroxide.

Fig. 7. Adsorption mechanism of phosphate [20,21].

an anion, the surface charge of the adsorbent must be controlled from the cation to the anion. PZC is one approach, but has a wide
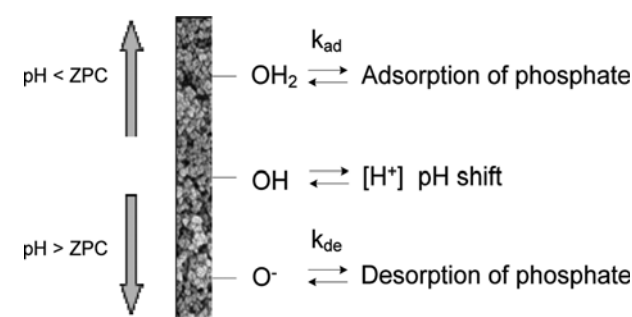
pH range. Accordingly, phosphate-adsorbed adsorbent must be changed from the cation to the anion to induce the repulsive force between the adsorbent and the adsorbed ion. The pH condition for the anion must be found throughout the experiment. Desorbed phosphate ion can be used in agriculture as a fertilizer and a conditioner of soils.

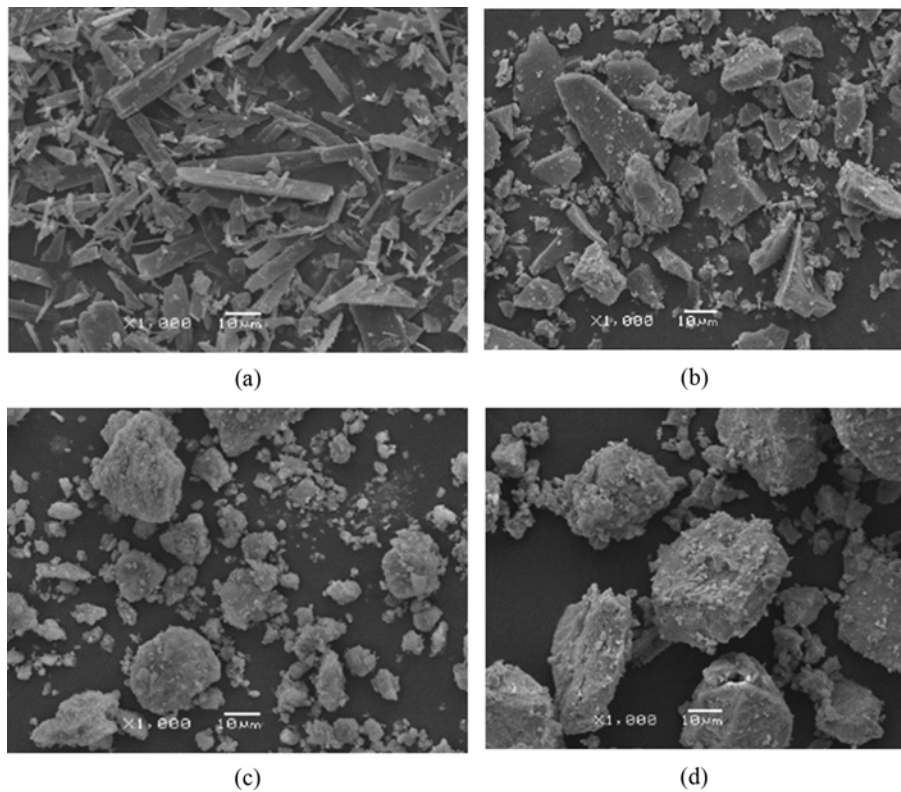One of the earliest adsorption models is that of James and

Fig. 8. SEM photos of samples synthesized by the change of pH conditions: (a) pH 3 (b) pH 6 (c) pH 9 (d) pH 13.

Healy [29], who proposed that the adsorption of hydrolysable metal cations was largely a physical process that could be described by an a priori calculation of the coulombic and solvation contributions to the adsorption free energy. Indeed, early qualitative studies of noble metal adsorption onto a support suggest that the principal attraction is electrostatic. Positively charged oxide surfaces (at pH<PZC) are capable of adsorbing anions, and negatively charged surfaces (at pH>PZC) are capable of adsorbing cations as shown in Fig. 7.

Fig. 8 shows the SEM photographs of the ferric hydroxides synthesized by changing the pH conditions. The SEM results showed that ferric hydroxide has a bar- or plate-type structure at pH 3 and an amorphous structure with irregular shapes in the case of pH 6. At pH 9 and pH 13, the particles had irregular and aggregated large sizes.

2. Performance Test

To date, phosphate adsorption experiments have been mainly conducted by using a batch-type adsorption performance test, as shown in Table 1. To compare the adsorption performance, batch-type adsorption experiment was carried out on the synthesized adsorbent. As the result, adsorption efficiency was obtained at 89% through the input of 1 g adsorbent to the solution of initial phosphate concentration of 300 ppm. The maximum adsorbed phosphate amount by the batch-type adsorption test was obtained by 130 mg phosphate/g adsorbent as shown in Fig. 9.

However, in practice, the batch-type adsorption method is difficult to apply in the field, such as in rivers and lakes, for the removal of phosphate. Accordingly, in this adsorption test, the phosphate
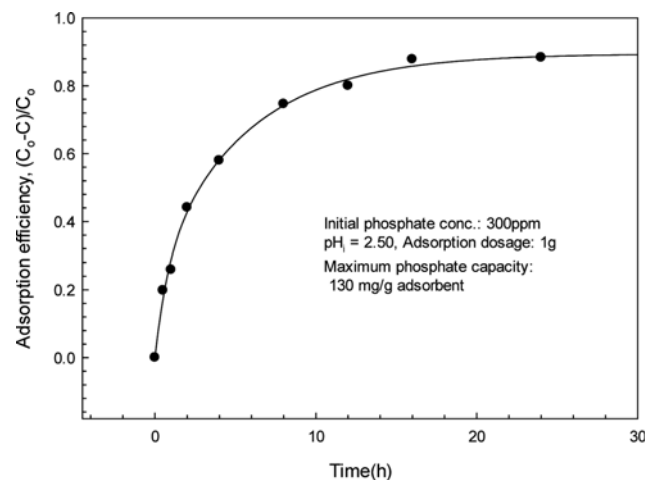

Fig. 9. Adsorption efficiency of initial phosphate concentration of 300 ppm on ferric hydroxide of 1.0 g by batch-type adsorption reactor.

solution was allowed to flow through the column naturally under gravity in the adsorption experiment. The applied column-type packed-bed adsorption apparatus was creatively designed to be able to support natural downward flow by gravity by considering a field environment similar to that found in natural rivers and lakes as shown in Fig. 2.

Fig. 10 shows the result of measuring the adsorption efficiency of phosphate analyzed using a column-type adsorption reactor on
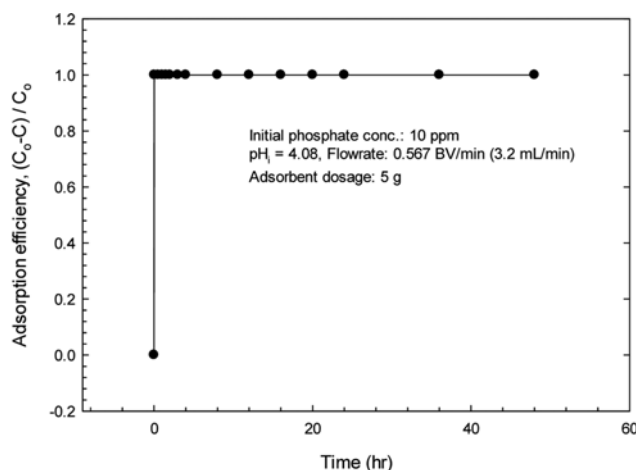
Fig. 10. Adsorption efficiency of initial phosphate concentration of 10 ppm at initial pH 4.08, 0.567 BV/min flow rate on ferric hydroxide adsorbent of 5 g by column-type adsorption reactor.

the ferric hydroxide synthesized at pH 6.

The phosphate concentration was analyzed by ICP-AES at different time intervals after the phosphate solution passed through the column. The amount of adsorbent added to the column was 5 g and the phosphate solution, which was obtained by dissolving phosphoric acid, was introduced at a flow rate of 0.567 BV/min. As the result of adsorption performance, the initial phosphate concentration of 10 ppm was completely adsorbed onto the ferric hydroxide adsorbent. Thus, the adsorption efficiency was 100% as the phosphate concentration was reduced from 10 ppm to 0 ppm within a period of 48 h.

The maximum adsorption capacity on 5 g of adsorbent was determined by introducing a phosphate solution of 100 ppm to the column. The result showed that the 100 ppm phosphate was completely adsorbed within the initial 3 h and then slowly reduced after
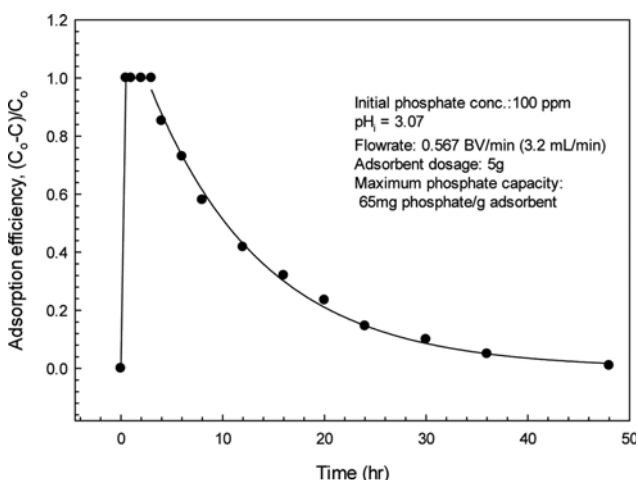

Fig. 11. Maximum adsorption capacity of initial phosphate concentration of 100 ppm at initial pH 3.07, 0.567 BV/min flow rate on 5 g ferric hydroxide adsorbent by column-type adsorption reactor.

3 h until 48 h as shown in Fig. 11.

The parameter for the f(t) equation shown in Fig. 11 is the result obtained by regressing the experimental f(t) data where the experimental data of f(t), were well fitted by the basic equation of

$f(t) = \int_{t_1}^{t_2} ae^{-bt} dt$ and then the established parameters of a=1.253, b=0.08918 were determined through regression. The equation was an exponential function with two parameters. On the other hand,

$f(t) = \int_{t_1}^{t_2} ae^{-bt} dt$ could easily be solved by using an integral formula

for the range from 3 h to 48 h.

The maximum adsorbed amount obtained as a result of the integration was calculated as 65 mg phosphate/g ferric hydroxide. This value was smaller than the maximum adsorbed amount of batch-type adsorption because the column-type has an inadequate residence times than the batch-type adsorption. Nonetheless, these values were very large maximum capacities compared to those of the adsorbents reported to date, as listed in Table 1.

CONCLUSIONS

A mesoporous adsorbent consisting of ferric hydroxide for the removal of phosphate was effectively synthesized from ferric sulfate discharged from the neodymium hydrometallurgical process. Effective adsorbent was synthesized by chemical treatment involving H_2O_2, aeration, and NaOH, and especially, the effect of various pH conditions was investigated. Ferric hydroxide with a high microstructure and amorphous structure was synthesized at pH 6. At this pH, a BET surface area of 194 m^2/g, pore volume of 0.129, average pore size of 2.7 nm, and PZC of 5.7, were obtained.

Previously, many studies conducted adsorption experiments by using a batch reactor, but our experiments used a creatively designed column-type packed-bed adsorption apparatus to enable flow by gravity in consideration of the natural field environment similar to that in natural rivers and lakes. The result of the column-type performance test indicated that a 10 ppm phosphate solution was completely adsorbed after passage through the adsorption column packed with 5 g of adsorbent within 2 min. Maximum adsorption efficiency of 100% was attained under the conditions of 0.567 BV/min flow rate and 298 K, and the maximum amount adsorbed was shown to be 65 mg/g adsorbent.

The adsorption characteristics of this adsorbent were excellent compared to the research results obtained in previous studies in terms of the cost, efficiency, contact time, and maximum adsorption capacity.

In conclusion, ferric hydroxide is an inexpensive and excellent adsorbent for the prevention of algal blooms and was effectively synthesized from the side product of a hydrometallurgical process. This adsorbent is expected to be an effective alternative to remove phosphate to prevent the occurrence of algal blooms.

ACKNOWLEDGEMENTS

REFERENCES

1. J. Huang, C. Xu, B. G. Ridoutt, X. Wang and P. Ren, *J. Cleaner Production*, **159**, 171 (2017).

2. M. West, N. Fenner, R. Gough and C. Freeman, *Ecological Engineering* (2017), DOI:10.1016/j.ecoleng.2017.07.033.

3. F. Xie, F. Wu, G. Liu, Y. Mu, C. Feng, H. Wang and J. P. Giesy, *Environ. Sci. Technol.*, **48**, 582 (2014).

4. Q. Liu, P. Hu, J. Wang, L. Zhang and R. Huang, *J. Taiwan Institute of Chemical Engineers*, **59**, 311 (2016).

5. M. Arshadi, S. Foroughifard, J. E. Gholtash and A. Abbaspourrad, *J. Colloid Interface Sci.*, **452**, 69 (2015).

6. G. Li, D. Chen, W. Zhao and X. Zhang, *J. Environ. Chem. Eng.*, **3**, 515 (2015).

7. M. E. Bouraie and A. A. Masoud, *Appl. Clay Sci.*, **140**, 157 (2017).

8. W. Xiong, J. Tong, Z. Yang, G. Zeng, Y. Zhou, D. Wang, P. Song, R. Xu, C. Zhang and M. Cheng, *J. Colloid Interface Sci.*, **493**, 17 (2017).

9. D. Mitrogiannis, M. Psychoyou, I. Baziotis, V. J. Inglezakis, N. Koukouzas, N. Tsoukalas, D. Palles, E. Kamitsos, G. Oikonomou and G. Markou, *Chem. Eng. J.*, **320**, 510 (2017).

10. C. Zhang, Y. Li, F. Wsng, Z. Yu, J. Wei, Z. Yang, C. Ma, Z. Li, Z. Xu and G. Zeng, *Appl. Surface Sci.*, **396**, 1783 (2017).

11. J. Dai, H. Yan, Y. Shangguan, Q. Zheng and R. Cheng, *Chem. Eng. J.*, **166**, 970 (2011).

12. Z. Ren, L. Shao and G. Zhang, *Water Air Soil Pollut.*, **223**, 4221 (2012).

13. J.-W. Choi, K.-S. Kwon, S. Lee, B. An, S.-W. Hong and S.-H. Lee, *Water Air Soil Pollut.*, **225**, 1835 (2014).

14. K. Wu, T. Liu, C. Ma, B. Chang, R. Chen and X. Wang, *Environ. Sci. Pollut. Res.*, **21**, 620 (2014).

15. S. H. Lee, S. W. Hing and J. W. Choi, *KIC News*, **14**, 22 (2011).

16. B. Beverskog and I. Puigdomenech, *Corrosion Science*, **38**, 2121 (1996).

17. P. Wilfert, P. S. Kumar, L. Korving, G.-J. Witkamp and M. C. M. van Loosdrecht, *Environ. Sci. Technol.*, **49**, 9400 (2015).

18. E. M. Michalos and A. A. Rouff, *Spectroscopy Lett.*, **48**, 695 (2015).

19. A. Munoz, F. M. Torres, J. M. Estela and V. Cerda, *Anal. Chim. Acta*, **350**, 21 (1997).

20. J. R. Regalbuto, A. Navada, S. Shadid, M. L. Bricker and Q. Chen, *J. Catal.*, **184**, 335 (1999).

21. W. A. Spieker and J. R. Regalbuto, *Chem. Eng. Sci.*, **56**, 3491 (2001).

22. X. Hao, W. A. Spieker and J. R. Regalbuto, *J. Colloid Interface Sci.*, **267**, 259 (2003).

23. K. B. Agashe and J. R. Regalbuto, *J. Colloid Interface Sci.*, **185**, 174 (1997).

24. W. A. Spieker, J. Liu, J. T. Miller, A. J. Kropf and J. R. Regalbuto, *Appl. Catal. A: Gen.*, **232**, 219 (2002).

25. W. A. Spieker, J. Liu, X. Hao, J. T. Miller, A. J. Kropf and J. R. Regalbuto, *Appl. Catal. A: Gen.*, **243**, 53 (2003).

26. J. S. Noh and J. A. Schwarz, *J. Colloid Interface Sci.*, **130**, 157 (1988).

27. J. R. Regalbuto, O. Ansel and J. T. Miller, *Topics in Catalysis*, **39**, 237 (2006).

28. J. Park and J. R. Regalbuto, *J. Colloid Interface Sci.*, **175**, 239 (1995).

29. R. O. James and T. W. Healy, *J. Colloid Interface Sci.*, **40**, 65 (1972).